RS•C
ROYAL SOCIETY OF CHEMISTRY

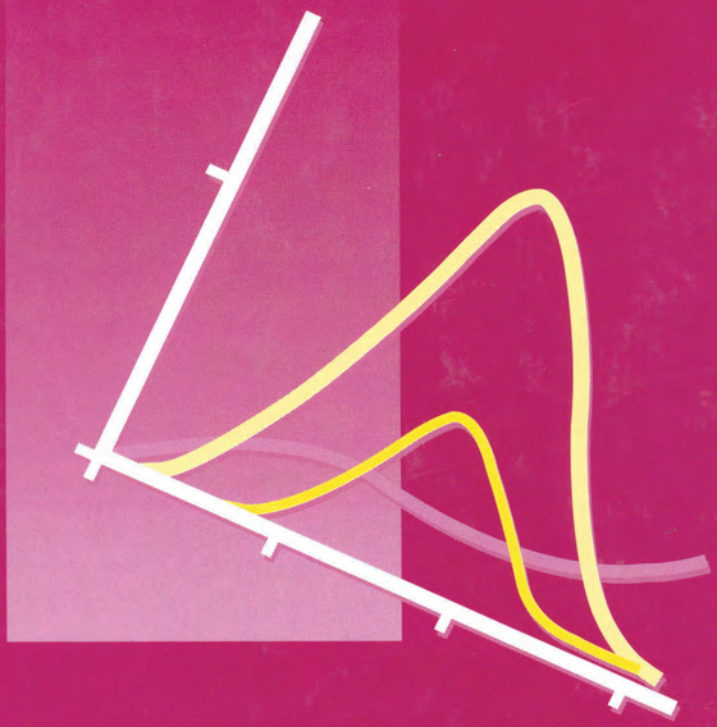

AN ATLAS OF *High Resolution Spectra of Rare Earth Elements for ICP-AES*

B. HUANG, X. WANG, P. YANG, H. YING,
S. GU, Z. ZHANG, Z. ZHUANG, Z. SUN, B. LI

An Atlas of High Resolution Spectra of Rare Earth Elements for Inductively Coupled Plasma Atomic Emission Spectroscopy

An Atlas of High Resolution Spectra of Rare Earth Elements for Inductively Coupled Plasma Atomic Emission Spectroscopy

Benli Huang, Xiaoru Wang, Pengyuan Yang,[1] Hai Ying, Sheng Gu, Zhigang Zhang, Zhixia Zhuang, Zhenhua Sun
Laboratory of Analytical Science for Material and Life Chemistry, Department of Chemistry, Xiamen University, Xiamen 361005, PR China

[1]Present address: Fudan University, Shanghai 200433, PR China

Bing Li
Institute of Rock and Mineral Analysis, Ministry of Geology and Mineral Resources, Beijing 100037, PR China

RS•C
ROYAL SOCIETY OF CHEMISTRY

ISBN 0-85404-477-9

A catalogue record for this book is available from the British Library

Published by The Royal Society of Chemistry,
Thomas Graham House, Science Park, Milton Road
Cambridge CB4 0WF, UK

For further information see our web site at www.rsc.org

Typeset by Paston PrePress Ltd, Beccles, Suffolk
Printed by Bookcraft (Bath) Ltd

Preface

Inductively coupled plasma atomic emission spectroscopy (ICP-AES) has moved into a period of rapidly growing application, as Prof. Fassel has pointed out. It has been widely adopted as a routine analytical technique for elemental analysis in various laboratories, companies and industries. As is always the case, the shortcomings of ICP-AES appeared gradually with its extensive application, one of which is spectral interference even with a high resolution spectrometer, especially for such line-rich elements as rare earth elements (REEs).

There is an old Chinese saying: 'A workman must first sharpen his tools if he wants to do his work well'. We hope that the present Altas is such a tool for analytical spectroscopists who want to determine the REEs well, and especially to determine them in REE matrices. The Atlas contains systematic, informative and useful data and profiles of high-resolution interferent spectra among REEs, especially the data of some newly proposed evaluation parameters. With the help of the Atlas, not only may the best analytical line(s) be selected with given matrices of REEs, but also a more comprehensive and complete understanding of the ICP may be obtained with the characteristics of the spectra.

The Atlas is composed of four parts. Part I is the Introduction, in which the aims of the book and the necessity of such research are clearly elucidated. Some concepts and principles used in the book are interpreted in detail. Conventional and more advanced criteria for evaluating spectral interference are illustrated with formulae and figures. The apparatus and the experimental procedures used are listed or described in detail. Many references published in the past are collected in Part II. The tables forming Part III contain the important data of the criteria for spectral coincidence profiles. The best analytical line(s) of a REE may be found directly from the tables for a particular REE matrix, or with some further simple calculation for a matrix of a particular mixture of REEs. The collection of coincidence profiles for a total of 65 prominent lines of 15 REEs which have not been adequately addressed previously in the literature are presented in Part IV. In addition to the hard copy of the coincidence profiles, an electronic version is provided on a compact disk supplied with this book. Instruction for use of the disk is included in the Appendix.

The authors gratefully acknowledge the support granted by the National Natural Science Foundation of China. They also sincerely appreciate the donation of the brand new ICP2070 spectrometer, especially equipped with a holographic grating of 3600 grooves/mm for the REEs, by Baird Corp., MA, USA, without which this Atlas could not have been produced.

Although the contents of this book have been examined and double-checked many times by the authors, referees, and editors, some errors will be inevitable. The authors would appreciate information concerning any errors.

Contents

SECTION I

Introduction

1 Overview

There is an increasing need for sensitive, accurate and convenient analytical techniques for analysis and determination of rare earth elements (REEs) with their expanding applications.[1] REEs are now widely used in various areas of industry, agriculture, material science and other modern technologies, for instance, special alloy steels, non-ferrous alloys, magnetic materials, fluorescent powders, various kinds of growth promotion fertilizer in agriculture, catalysts in oil refining, additives in new ceramic materials, *etc.*

Being a powerful tool for elemental analysis, inductively coupled plasma atomic emission spectroscopy (ICP-AES) plays a more and more important role in the purity analysis of REEs owing to its high performance, such as: low detection limits ($< 0.0x\ \mu g\ ml^{-1}$), good precision, wide linear dynamic range, simple sample treatment, *etc.* As shown in many papers, ICP-AES has the potential to determine individual REEs directly without mutual separation,[2] provided the spectrometer has adequate resolution and dispersion.

However, one of the basic problems of AES is spectral interference from the concomitant and matrix elements of the sample. In addition, REEs are well-known spectral line-rich elements. Improper analytical line selection may result in significant loss of detection power or accuracy for samples containing REE matrices. Therefore, it is crucial to choose appropriate analytical lines in order to avoid interference and ensure the quality of analysis.[3] It is obvious that the line coincidence atlases are always the most emphasized and important fundamental research for ICP-AES, as stressed by many spectrochemists at a workshop held in Scarborough, Ont., Canada, in 1987: *Needs for Fundamental Atomic Reference Data for Analytical Spectroscopy, Spectrochim. Acta, Part B, 1988,* **43**, No. 1.[4]

Although quite a few extensive tables[5–19] have been published for REEs, few of them meet the demands for optimum selection of analytical line(s) for samples with REEs as major constituents. Some of them lack the mutual interferent information among the REE lines, and most of them do not provide spectral coincidence profiles. For those atlases with spectral profiles, the overlay information is still insufficient or not so accurate owing to the use of a low-resolution spectrometer for obtaining the spectral information. Many weak lines of REEs are missed or submerged in profiles of other sensitive lines. Furthermore, the general assessments adopted for rational line selection were

sensitivity, detection limit, and signal-to-background ratio (SBR), *etc.* Another significant criterion for selecting analytical line(s), the true detection limit proposed by Boumans,[11] has not been applied in most of these atlases.

The aim of this atlas is to provide spectral interference data for REEs, with emphasis on the spectral interferences occurring among REEs themselves.[20–22] The atlas will cover the following aspects:

1. to record the detailed spectra of all REEs in the wavelength region adjacent to each of the prominent lines of a particular REE with a high-resolution ICP-AES instrument;
2. to provide reliable evaluation, based on recorded spectra, of the powers of detection of the chosen prominent lines for samples with the matrices of the other REEs;
3. to recommend the best analytical line(s) of an analyte with less interference and higher sensitivities for analysis with a particular REE matrix;
4. to provide data for calculating the criteria to choose the best line(s) with mixed REEs matrices.

2 Interpretation

Spectral Coincidence Profiles

Spectral coincidence profiles, according to our experience, are the simplest and clearest illustration for interpreting the interfering spectra. The graphic format not only provides us with the interference data, but also gives us a visual impact of the spectra in a certain wavelength range, from which we could obtain information on different kinds of interference, such as direct overlap, wing overlap and line broadening interference.

The coincidence profiles are presented in Part IV. These profiles for each prominent line are divided into four separate plots, each of them consisting of linear-scaled profiles of analyte spectral profile superimposed with interferent profiles La, Ce, Sm, Dy in plot A, Er, Ho, Tb, (Dy) in plot B, Eu, Gd, Lu, Tm in plot C, and Nd, Pr, Y, Yb in plot D, respectively. The magnitude of an interference can be estimated by a simple comparison of the analyte and interferent intensities at the analytical wavelength. The wavelengths of some unlabelled interferent lines in the plots may be found in the Tables of Interfering Lines in Part III. The full view of the spectra can be zoomed with programs on the disk enclosed with this book. This is especially useful for those profiles in which the analyte and interferent peaks are of significantly different magnitude.

Detection Limits

Detection limits (C_L) in ICP-AES are usually defined as the concentrations that yield a net line signal equal to an arbitrary factor (K) times the relative standard deviation (σ_B) of the background signal (X_B):

$$C_L = \frac{K \cdot \sigma_B \cdot X_B}{S_A} \tag{I-1}$$

where

$$S_A = \frac{X_A}{C_A} \tag{I-2}$$

S_A: sensitivity of analyte;
X_A: the net analyte signal;
C_A: the analyte concentration to produce X_A.

Commonly, the relative standard deviation of the background σ_B is conservatively assumed to be 0.01. However, various values of K have been used by different workers. By convention, K is equal to 3, which corresponds approximately to 95% confidence. In the definition of the conventional detection limit given by Boumans in case of interference, K is equal to $2\sqrt{2}$. Here, in order to be consistent with other literature, a value of 3 is used for K. Therefore, the detection limit may be written as:

$$C_L = \frac{0.03 \cdot X_B}{S_A} = \frac{0.03 \cdot C_A}{X_A/X_B} = \frac{0.03 \cdot C_A}{SBR} \tag{I-3}$$

Background Equivalent Concentration

Background equivalent concentration (BEC) is usually defined as the concentration that yields a net line signal equal to the net solvent blank signal, which may be estimated as:

$$\mathrm{BEC} = \frac{X_B}{S_A} \tag{I-4}$$

BEC is another empirical evaluation of detection power of the analysis.

True Detection Limit and Q Values

True detection limit ($C_{L,true}$) assessment was proposed by Boumans and Vrakking for rational selection of wavelength lines. It has been proved capable to be a simple, applicable and standard criterion for estimating the type and magnitude of spectral interference in the analysis of real samples.

According to Ref. 11, for a multi-component system, in case of interference, $C_{L,true}$ is defined as:

$$C_{L,true} = \frac{2}{5}\sum_j \frac{S_{I,j}(\lambda_a)}{S_A} C_{I,j} + C_{L,conv} \tag{I-5}$$

where λ_a: the peak wavelength of an analysis line;

$S_{I,j}(\lambda_a)$: the sensitivity of component j at the interfering line at λ_a;
S_A: sensitivity of analyte;
$C_{I,j}$: the interferent concentration of component j;
$C_{L,conv}$: the conventional detection limit.

The conventional detection limit can be written as:

$$C_{L,conv} = 2\sqrt{2} \times 0.01 \times RSDBl \times \frac{X_{BL}}{S_A} \tag{I-6}$$

in which, $RSDBl$ (%) is the relative standard deviation of the total background signal X_{BL}, which is written as:

$$X_{BL} = X_B + \sum_j X_{I,j} + \sum_j X_{W,j} \tag{I-7}$$

where X_B: the net background signal at λ_a;
$X_{I,j}$: the net interferent signal of component j at λ_a;
$X_{W,j}$: the net wing signal of component j at λ_a;

So the ratio X_{BL}/S_A may be written as:

$$\frac{X_{BL}}{S_A} = \frac{X_B}{S_A} + \sum_j \frac{S_{I,j}(\lambda_a)}{S_A} C_{I,j} + \sum_j \frac{S_{W,j}(\Delta\lambda_a)}{S_A} C_{I,j} \tag{I-8}$$

Boumans thinks that the quotients of $S_{I,j}$ and $S_{W,j}$ with S_A are more meaningful than the values themselves:

$$Q_{I,j}(\lambda_a) = \frac{S_{I,j}(\lambda_a)}{S_A} \tag{I-9}$$

$$Q_{W,j}(\Delta\lambda_a) = \frac{S_{W,j}(\Delta\lambda_a)}{S_A} \tag{I-10}$$

The Q values are more convenient and have universal significance in that they are independent of (a) the transmission characteristics of the spectrometer and the response characteristic of the detector; (b) the transport efficiency of the nebulizer, at least to a first approximation; and (c) the units in which the sensitivities are expressed.

Then the conventional detection limit is obtained:

$$C_{L,conv} = 2\sqrt{2} \times 0.01 \times RSDBl \times \left[BEC + \sum_j Q_{I,j}(\lambda_a) C_{I,j} + \sum_j Q_{W,j}(\Delta\lambda_a) C_{I,j} \right] \tag{I-11}$$

Finally, we have

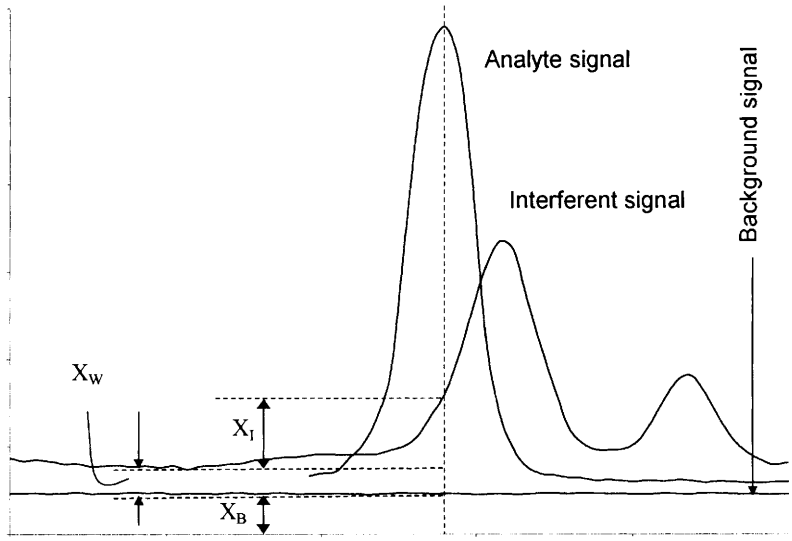

Figure I-1 *Illustration of X_B, X_I, and X_W*

$$C_{\mathrm{L,true}} = \frac{2}{5}\sum Q_{\mathrm{I},j}(\lambda_{\mathrm{a}})C_{\mathrm{I},j} + 2\sqrt{2} \times 0.01 \times RSDBl \times \left[BEC + \sum_j Q_{\mathrm{I},j}(\lambda_{\mathrm{a}})C_{\mathrm{I},j} + \sum_j Q_{\mathrm{W},j}(\Delta\lambda_{\mathrm{a}})C_{\mathrm{I},j}\right] \quad \text{(I-12)}$$

The basic parameters, X_{B}, X_{I}, and X_{W}, are illustrated in Figure I-1.

3 Apparatus and Procedures

Apparatus

A commercial sequential high-resolution ICP-AES spectrometer was employed for collection of the coincidence profiles. The specification of the instrument and the optimized operating conditions are summarized in Table I-1.

Sample Solutions

The stock solutions ($1\,\mathrm{mg\,ml^{-1}}$) were provided by Shanghai Institute of Material Science (spectral purity >99.995%). The standard solution and the artificial 'pure' matrix solution of each rare earth element (listed in Table I-2) were prepared by diluting the stock solutions with distilled and deionized water prepared by the MilliQ water purification system. For example, 1 ml Ce standard solution ($1\,\mathrm{mg\,ml^{-1}}$) and 10 ml nitric acid (AR) were mixed and diluted to 200 ml to obtain the analytical standard solution. The final concentration of HNO_3 in all test solutions was $0.8\,\mathrm{mol\,l^{-1}}$. $0.8\,\mathrm{mol\,l^{-1}}$ nitric acid prepared with distilled and deionized water was used as the blank solution.

Table I-1 *Instrumentation and optimized operating conditions*

Model 2070 ICP-AES spectrometer (Baird Corp., 125 Middlesex Turnpike, Bedford, MA 01730, USA)	
Monochromator	1 m vacuum, C-T mounting 1 cm foam lining added to thermostatic housing
Grating	3600 groves mm^{-1}, holographic
Scanning mechanism	Harmonic drive
Entrance and Exit Slit widths	17.5 μm
Bandpass (FWHM)	0.007 nm
Detectors	Two selected PMTs: UV 160–290 nm VIS 290–900 nm PMT Gain 6
RF Generator power	40.68 MHz, crystal controlled. Solid state, computer controlled with an automatic matching network
Forward power	1050 W
Reflected power	2 W
Torch	One-piece quartz, low flow design
Sample introduction	Concentric pneumatic glass nebulizer, Scott-type glass spray chamber, peristaltic pump
Argon gas flow rates	Outer gas flow rate 9 l min^{-1} Intermediate gas flow rate 0.85 l min^{-1} Carrier gas inlet pressure 32 psi
Solution uptake rate	1.50 ml min^{-1}

Table I-2 *The concentrations of the adopted standard solutions and matrix solutions*

	Concentration (μg ml^{-1})	
Element	*In standard solution*	*In matrix solution*
La	5	1000
Ce	5	1000
Pr	10	100
Nd	5	100
Sm	5	1000
Eu	1	100
Gd	5	100
Tb	5	1000
Dy	5	1000
Ho	1	1000
Er	1	1000
Tm	1	100
Yb	1	100
Lu	1	100
Y	1	100

Selection of Prominent Lines

Consulting other references, lines with large signal to background ratio (S/B) were selected for the present study. In this work, four to six prominent analytical lines were selected to investigate the spectral interference for each rare earth element. The detection limits of the selected prominent lines of each REE obtained by the authors are listed in Table III-1.

Experimental Procedures

As indicated in the section on Sample Solutions, the blank, standard and 'pure' matrix solutions were used to obtain the spectral data of background, analytes, and matrices respectively. The window width of the sequential spectrometer used in this study was set to 0.2 nm. Within the 0.2 nm window, every spectrum of background, analytes, and matrices was recorded in steps of approximate 0.9 pm. The integration time is 0.2 s per step with a constant voltage setting for the photomultiplier (PMT). Under these conditions, there are more than 200 measurement points per scan and 15 scans per profile for each of the 65 spectral lines. Thus, approximately 198 000 intensity measurements for the coincidence profiles have been made.

The coincidence profiles were obtained by superimposing the profiles of signals of background, analyte, and matrices that were located in the same wavelength range. In addition to the visualization of interference, the relevant criteria, C_L, $C_{L,conv}$, $C_{L,true}$ and Q values may be finally determined. A computer program compiled by the authors was used to locate positions of peaks and to calculate these critera automatically. Readers may contact the authors if they are interested in this program.

To maintain the excitation conditions consistent, the intensities of Dy II 364.540 nm and Sm II 359.260 nm were checked every working day with 5 $\mu g\,ml^{-1}$ of standard solution under the optimum conditions. If the intensities of those lines monitored were out of the tolerance range, the carrier gas flow rate was adjusted to maintain the initial intensities. When investigation for one matrix spectrum was completed, the plasma torch and nebulizer were cleaned thoroughly with concentrated nitric acid (50%) to avoid memory effects.

Wavelength Accuracy and Reproducibility

Wavelength accuracy and reproducibility are decisive to the superimposibility of the coincidence profiles. The grating drive mechanism of the ICP 2070 is based on a harmonic drive. It works with a tolerance, reported by the instrument manufacturer, of less than one step. Consequently, the accuracy of the peak position located should be less than two steps, *i.e.* 1.8 pm. From the wavelength range of 200–500 nm, a prominent line of a known element was selected to check the shift of the grating position for about every 40 nm. For instance, Cu (1 $\mu g\,ml^{-1}$) II 213.598 nm and Lu (1 $\mu g\,ml^{-1}$) II 307.760 nm were used in the corresponding windows for such calibration purposes in this work.

The experimental results show that the shifts are actually less than ± 2 pm for five individual scans of the same line. Therefore the accuracy of the estimated wavelength for a peak in replicated scan should be less than ± 5 pm.

SECTION II

References

1. Sheng Gu, Hai Ying, Zhigang Zhang, Zhixia Zhuang, Pengyuan Yang, Xiaoru Wang, Benli Huang and Bing Li, *Spectrochimica Acta*, 1997, **52B**, 1567.
2. Y. Nakamura, K. Takahashi, O. Kujirai and H. Okochi, *J. Anal. Atom. Spectrosc.*, 1990, **5**, C3155.
3. S.R. Marin, S.G. Cornejo and L. Arriagada, *J. Anal. Atom. Spectrosc.*, 1994, **9**, 93.
4. P.W.J.M. Boumans and A. Scheeline, Eds., Proceedings of a Workshop: 'Need for Fundamental Atomic Reference Data for Analytical Spectroscopy', *Spectrochim. Acta*, 1988, **43B**, No.1 (Special Issue).
5. Aili Pei, Lianfang Shen, Jianhua Chen, Yuanzhu Ouyang, Benli Huang, Dingzhao Zhang, *An Atlas of Spectra of Mixtures of Rare Earth Elements*, Science Press, Beijing, 1964 (in Chinese).
6. Zhenpeng Qian, Changqin Wang, Weihua Chen, *An Atlas of Spectra of Rare Earth Elements for ICP-AES*, Metallurgical Industry Press, Beijing, 1984 (in Chinese).
7. Deren Qiu, Wanxia Chen, *Spectral Line Tables for a 2 Å/mm and 4 Å/mm Grating Spectrograph*, Shanghai Science and Technology Press, Shanghai, 1984 (in Chinese).
8. M.L. Parsons, A. Foster and D. Anderson, *An Atlas of Spectral Interference in ICP Spectroscopy*, Plenum Press, New York and London, 1980.
9. R.W. Winge, V.A. Fassel, V.J. Peterson and M.J. Floyd, *Inductively Coupled Plasma Atomic Emission Spectroscopy – An Atlas of Spectral Information*, Elsevier, Amsterdam, 1985.
10. P.W.J.M. Boumans, *Line Coincidence Tables for Inductively Coupled Plasma Atomic Emission Spectrometry, Vols. I and II*, Pergamon Press, New York, 1980.
11. P.W.J.M. Boumans, J.A. Tielooy and F.J.M.J. Maessen, *Spectrochim. Acta*, 1988, **43B**, 173.
12. P.W.J.M. Boumans J.J.A.M. Vrakking and A.H.M. Heijms, *Spectrochim. Acta*, 1988, **43B**, 1365.
13. P.W.J.M. Boumans, He Zhizhuang, J.J.A.M. Vrakking, J.A. Tielrooy and F.J.M.J. Maessen, *Spectrochim. Acta*, 1989, **44B**, 31.
14. V. Kanick and J. Toman, *ICP Information Newsletter*, 1990, **15**, 444.
15. N. Daskalova, S.Velichkov, N. Krasnobaeva and P. Slavova, *Spectrochim. Acta*, 1992, **47B**, 1595.
16. N. Daskalova, S.Velichkov and P. Slavova, *Spectrochim. Acta*, 1992, **48B**, 1743.
17. A.A. Ghazi, S. Qamar and M.A. Atta, *Spectrochim. Acta*, 1993, **48B**, 1107.
18. A.A. Ghazi, S. Qamar and M.A. Atta, *Spectrochim. Acta*, 1994, **49B**, 527.
19. A.A. Ghazi, S. Qamar and M.A. Atta, *ICP Information Newsletter*, 1995, **20**, 627.
20. Bing Li, Min Yi, Zhigang Zhang, Xiaoru Wang, Pengyuan Yang, Zhixia Zhuang, and Benli Huang, *Fenxi Yiqi Ceshi Tongxun (Analytical Instruments Newsletter)*, 1996, **61**, 63 (in Chinese).

21. Sheng Gu, Pengyuan Yang, Bing Li, Zhigang Zhang, Xiaoru Wang, *Guangpuxue yu Guanpu Fenxi (Spectroscopy and Spectral Analysis)*, 1997, **17** (2), 88 (in Chinese).
22. Hai Ying, Pengyuan Yang, Zhigang Zhang, Sheng Gu, Xiaoru Wang and Benli Huang, *Guangpuxue yu Guanpu Fenxi (Spectroscopy and Spectral Analysis)*, 1998, **18** (5), 559 (in Chinese).

SECTION III

Coincidence Tables (Alphabetical Listing by Elements)

Table III-1 *Selected prominent lines of REEs and their detection limits and BECs obtained in the present work*

Element	*Wavelength* (nm)	*BEC* ($\mu g\ ml^{-1}$)	*CL* ($\mu g\ ml^{-1}$)	*Element*	*Wavelength* (nm)	*BEC* ($\mu g\ ml^{-1}$)	*CL* ($\mu g\ ml^{-1}$)
Ce II	413.765	0.36	0.012	Lu II	261.542	0.0056	0.00017
Ce II	413.380	0.32	0.010	Lu II	291.139	0.062	0.0020
Ce II	418.660	0.31	0.010	Lu II	219.554	0.064	0.0021
Ce II	395.254	0.78	0.023	Lu II	307.760	0.065	0.0021
Ce II	399.924	0.54	0.016	Nd II	401.225	0.25	0.0078
Ce II	446.021	0.45	0.015	Nd II	430.358	0.41	0.013
Dy II	353.170	0.045	0.0014	Nd II	406.109	0.31	0.010
Dy II	364.540	0.130	0.004	Nd II	415.608	0.54	0.018
Dy II	340.780	0.182	0.057	Nd II	386.340	0.59	0.018
Dy II	353.602	0.170	0.0053	Nd II	410.946	0.41	0.012
Er II	337.271	0.055	0.0018	Pr II	390.844	0.56	0.018
Er II	349.910	0.095	0.0032	Pr II	414.311	0.72	0.023
Er II	323.058	0.120	0.0041	Pr II	417.939	0.78	0.025
Er II	326.478	0.128	0.0044	Pr II	422.535	0.80	0.026
Eu II	381.967	0.023	0.0007	Sm II	359.260	0.19	0.006
Eu II	412.970	0.046	0.0014	Sm II	442.434	0.33	0.011
Eu II	420.505	0.057	0.0018	Sm II	360.949	0.25	0.0079
Eu II	393.048	0.050	0.0016	Sm II	363.429	0.38	0.012
Gd II	342.247	0.087	0.0027	Tb II	350.917	0.200	0.0063
Gd II	336.223	0.150	0.0046	Tb II	384.873	0.534	0.018
Gd II	335.047	0.126	0.0039	Tb II	367.635	0.416	0.014
Gd II	335.862	0.186	0.0058	Tb II	387.417	0.66	0.023
Ho II	345.600	0.103	0.0034	Tm II	313.126	0.045	0.0014
Ho II	339.898	0.226	0.0088	Tm II	346.220	0.058	0.0018
Ho II	389.102	0.289	0.012	Tm II	384.802	0.072	0.0023
Ho II	347.426	0.277	0.011	Tm II	342.508	0.079	0.0026
La II	333.749	0.079	0.0024	Y II	371.030	0.011	0.00034
La II	379.478	0.064	0.0019	Y II	324.228	0.018	0.00056
La II	408.672	0.084	0.0026	Y II	360.073	0.016	0.00049
La II	412.323	0.083	0.0025	Y II	377.433	0.016	0.00047
La II	398.852	0.17	0.0052	Yb II	328.937	0.0063	0.00019
				Yb II	369.419	0.0114	0.00034
				Yb II	289.138	0.045	0.0014
				Yb II	222.446	0.049	0.0015

Table III-2.1 *Tables of interfering lines of the other REEs matrices adjacent to the prominent line Ce II 395.254 nm*

Analyte: Ce
Prominent line: 395.254 nm

Element	*Wavelength* (nm)	$\Delta\lambda_{ka}$ (pm)
Dy	395.175	−79
	395.192	−62
	395.202	−52
	395.244	−10
	395.256	+2
	395.260	+6
	395.281	+27
	395.312	+58
Er	395.174	−80
	395.184	−70
	395.252	−2
	395.263	+9
	395.293	+39
Eu	395.249	−5
	395.345	+91
Gd	395.198	−56
	395.241	−13
	395.257	+3
	395.308	+54
	395.345	+91
Ho	395.211	−43
	395.266	+12
	395.286	+32
	395.303	+49
La	395.339	+85
Lu		
Nd	395.173	−81
	395.183	−71
	395.215	−39
	395.227	−27
	395.241	−13
	395.248	−6
	395.266	+12
	395.282	+28
	395.300	+46
	395.338	+84
	395.350	+96
Pr	395.178	−76
	395.193	−61
	395.215	−39
	395.232	−22
	395.245	−9
	395.288	+34
	395.305	+51
	395.312	+58
	395.350	+96
	395.357	+103
Sm	395.163	−91
	395.167	−87
	395.189	−65
	395.213	−41
	395.232	−22
	395.240	−14
	395.263	+9
	395.290	+36
	395.316	+62
	395.333	+79
Tb	395.170	−84
	395.186	−68
	395.211	−43
	395.239	−15
	395.257	+3
	395.285	+31
	395.298	+44
	395.311	+57
	395.337	+83
Tm		
Y		
Yb		

Table III-2.2 *Tables of interfering lines of the other REEs matrices adjacent to the prominent line Ce II 399.924 nm*

Analyte: Ce
Prominent line: 399.924 nm

Element	*Wavelength* (nm)	$\Delta\lambda_{ka}$ (pm)
Dy	399.841	−83
	399.858	−66
	399.891	−33
	399.913	−11
	399.923	−1
	399.934	+10
	399.963	+39
	399.982	+58
	399.998	+74
Er	399.920	−4
	399.932	+8
	399.954	+30
	400.010	+86
Eu	399.847	−77
	399.882	−42
	399.950	+26
	399.999	+75
Gd	399.916	−8
	399.961	+37
	400.000	+76
Ho	399.837	−87
	399.877	−47
	399.884	−40
	399.911	−13
	399.947	+23
	399.964	+40
La		
Lu		
Nd	399.820	−104
	399.838	−86
	399.850	−74
	399.873	−51
	399.913	−11
	399.924	+0
	399.940	+16
	399.951	+27
	399.982	+58
	399.998	+74
Pr	399.829	−95
	399.839	−85
	399.858	−66
	399.870	−54
	399.876	−48
	399.915	−9
	399.922	−2
	399.928	+4
	399.962	+38
	399.988	+64
Sm	399.835	−89
	399.849	−75
	399.864	−60
	399.885	−39
	399.905	−19
	399.936	+12
	399.957	+33
	399.969	+45
	399.989	+65
	400.015	+91
	400.022	+98
Tb	399.830	−94
	399.863	−61
	399.876	−48
	399.921	−3
	399.935	+11
	399.956	+32
	399.993	+69
Tm		
Y		
Yb		

Table III-2.3 *Tables of interfering lines of the other REEs matrices adjacent to the prominent line Ce II 413.380 nm*

Analyte: Ce
Prominent line: 413.380 nm

Element	*Wavelength* (nm)	$\Delta\lambda_{ka}$ (pm)
Dy	413.294	−86
	413.321	−59
	413.335	−45
	413.351	−29
	413.386	+6
	413.414	+34
	413.444	+64
	413.475	+95
Er	413.340	−40
	413.395	+15
	413.402	+22
	413.461	+81
	413.477	+97
Eu	413.314	−66
	413.342	−38
	413.408	+28
	413.416	+36
Gd	413.316	−64
	413.349	−31
	413.416	+36
Ho	413.323	−57
	413.388	+8
	413.412	+32
	413.439	+59
	413.451	+71
	413.486	+106
La	413.331	−49
Lu		
Nd	413.299	−81
	413.312	−68
	413.333	−47
	413.351	−29
	413.369	−11
	413.399	+19
	413.430	+50
	413.438	+58
	413.440	+60
	413.449	+69
	413.476	+96
Pr	413.291	−89
	413.315	−65
	413.323	−57
	413.362	−18
	413.384	+4
	413.395	+15
	413.422	+42
	413.429	+49
	413.446	+66
	413.453	+73
	413.470	+90
	413.483	+103
Sm	413.319	−61
	413.359	−21
	413.372	−8
	413.388	+8
	413.405	+25
	413.428	+48
	413.450	+70
	413.478	+98
Tb	413.313	−67
	413.319	−61
	413.341	−39
	413.362	−18
	413.403	+23
	413.429	+49
Tm	413.324	−56
	413.444	+64
Y		
Yb	413.446	+66

Table III-2.4 *Tables of interfering lines of the other REEs matrices adjacent to the prominent line Ce II 413.765 nm*

Analyte: Ce
Prominent line: 413.765 nm

Element	*Wavelength* (nm)	$\Delta\lambda_{ka}$ (pm)	*Element*	*Wavelength* (nm)	$\Delta\lambda_{ka}$ (pm)
Dy	413.667	−98	Nd	413.670	−95
	413.689	−76		413.688	−77
	413.737	−28		413.707	−58
	413.760	−5		413.730	−35
	413.774	+9		413.749	−16
	413.794	+29		413.759	−6
	413.828	+63		413.781	+16
	413.854	+89		413.801	+36
				413.812	+47
Er	413.665	−100		413.832	+67
	413.702	−63		413.846	+81
	413.717	−48			
	413.727	−38	Pr	413.692	−73
	413.771	+6		413.713	−52
	413.804	+39		413.753	−12
	413.853	+88		413.769	+4
				413.775	+10
Eu	413.722	−43		413.784	+19
	413.761	−4		413.793	+28
	413.817	+52		413.814	+49
Gd	413.704	−61	Sm	413.665	−100
	413.761	−4		413.686	−79
	413.810	+45		413.699	−66
	413.846	+81		413.729	−36
				413.768	+3
Ho	413.679	−86		413.794	+29
	413.694	−71		413.815	+50
	413.748	−17		413.835	+70
	413.776	+11		413.850	+85
	413.801	+36			
	413.826	+61	Tb	413.703	−62
				413.727	−38
La	413.703	−62		413.787	+22
	413.793	+28		413.795	+30
				413.814	+49
Lu	413.706	−59		413.828	+63
	413.743	−22		413.849	+84
			Tm	413.748	−17
				413.771	+6
				413.793	+28
				413.835	+70
			Y	413.809	+44
			Yb		

Table III-2.5 *Tables of interfering lines of the other REEs matrices adjacent to the prominent line Ce II 418.660 nm*

Analyte: Ce
Prominent line: 418.660 nm

Element	*Wavelength* (nm)	$\Delta\lambda_{ka}$ (pm)	*Element*	*Wavelength* (nm)	$\Delta\lambda_{ka}$ (pm)
Dy	418.607	−53	Nd	418.663	+3
	418.639	−21		418.675	+15
	418.657	−3		418.689	+29
	418.682	+22		418.704	+44
	418.695	+35		418.714	+54
	418.715	+55		418.725	+65
	418.737	+77		418.755	+95
Er	418.598	−62	Pr	418.576	−84
	418.617	−43		418.610	−50
	418.635	−25		418.629	−31
	418.674	+14		418.654	−6
	418.698	+38		418.670	+10
	418.724	+64		418.682	+22
				418.693	+33
Eu	418.632	−28		418.706	+46
	418.648	−12		418.740	+80
	418.693	+33		418.770	+110
	418.699	+39			
	418.737	+77	Sm	418.566	−94
	418.754	+94		418.588	−72
				418.605	−55
Gd	418.646	−14		418.627	−33
	418.660	0		418.646	−14
	418.689	+29		418.658	−2
	418.721	+61		418.663	+3
				418.680	+20
Ho	418.596	−64		418.703	+43
	418.610	−50		418.725	+65
	418.638	−22		418.756	+96
	418.649	−11			
	418.656	−4	Tb	418.586	−74
	418.671	+11		418.626	−34
	418.685	+25		418.663	+3
	418.694	+34		418.699	+39
	418.702	+42		418.716	+56
	418.713	+53		418.736	+76
La	418.732	+72	Tm	418.638	−22
				418.698	+38
Lu	418.682	+22			
	418.699	+39	Y	418.632	−28
				418.689	+29
Nd	418.586	−74		418.734	+74
	418.603	−57			
	418.611	−49	Yb	418.682	+22
	418.624	−36		418.690	+30
	418.644	−16		418.709	+49
	418.647	−13			